# Photogrammetric calibration and accuracy evaluation of a cross-pattern stripe projector

Claus Brenner[a], Jan Böhm[b] and Jens Gühring[c]

Institute for Photogrammetry, University of Stuttgart

## ABSTRACT

Presently there is a growing demand for fast and precise 3D computer vision systems for a wide variety of industrial applications like reverse engineering, quality control and industrial gauging. One important aspect of any vision system is the data acquisition. If the principle of triangulation is used the correspondence problem is to be solved. The coded light approach offers a fast way to overcome this problem and to provide dense range data. In order to get high accuracy range images the system needs to be calibrated. In this paper, we compare two calibration techniques: polynomial depth calibration and photogrammetric calibration. We have carried out both methods independently. To obtain results about the accuracy in object space, we measured the surface of a plane-table.

**Keywords:** Calibration, coded light system, bundle adjustment, range sensor, 3D surface measurement

## 1. INTRODUCTION

The industrial image processing sector is booming. After a startup phase it becomes now clear that a lot of companies have developed appropriate hardware and software which can be used in a wide range of industrial inspection tasks. The market is driven by the need for more productivity, which results in automated production lines and a drive for quality improvement, partly caused by the demand for a 100% quality control. Nevertheless, it can be observed that most inspection tasks today involve the processing of 2D data only. Typical examples are checking if caps are present and in the right position, inspection of screws, measurement of flat punched steel and tasks involving a check for completeness of objects. Indeed, problems are so standardized that several "smart cameras" are on the market which can do the appropriate calculations without the need for external computing power. The ongoing revolution in the CMOS image sensor business will finally yield systems essentially consisting of one single imaging and processing chip. However, "measurement" nowadays most often means checking of dimensions in the image coordinate system. Correct dimensions are teached in terms of image coordinates by presenting a reference part to the system. No explicit 3D modeling and calibration is done.

Optical measurement techniques are ideally suited for 3D inspection and gauging tasks because of their ability to measure a wide range of objects and to deliver dense measurement data of some 100,000 points in a matter of seconds. Thus, it becomes possible to use those techniques for quality control of even inexpensive parts, which is not feasible using conventional coordinate measurement machines. Evaluation of 3D data is easier compared to grayvalue image data because geometry information is contained explicitly in the data. Dense 3D measurements still need a large amount of storage space and computing power, but the situation has improved considerably due to the availability of inexpensive PC's. All those prospects have led to the vision of an optical "multi-eyed measurement robot"[1] capable of inspecting parts fully automatically.

Nevertheless, it has to be noted that even some years after this vision, photogrammetry is still confined mostly to a small range of applications in the aircraft, aerospace, telescope and shipbuilding industry. There, most of the jobs consist of 3D point determination of signalized points.[2] Besides this, there are niche applications like the dense digitization of car bodies and design models, where automated image matching algorithms are used successfully.[3,4]

Since development cycles are becoming faster, more and more industrial parts are constructed in less time. Additionally, many parts nowadays are constructed using 3D CAD systems. Thus, it becomes time critical to deliver means for quality control. Instead of using specially prepared gauges it would be more economical to have 3D

Address: [a,b,c]Institute for Photogrammetry, University of Stuttgart, P.O.B. 106037, 70049 Stuttgart / Germany.

Email: [a]claus.brenner@ifp.uni-stuttgart.de, [b]jan.boehm@ifp.uni-stuttgart.de, [c]jens.guehring@ifp.uni-stuttgart.de

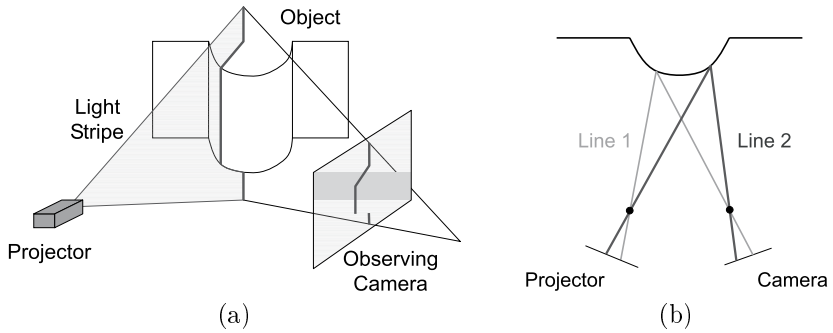


**Figure 1.** (a) Standard light sectioning with one light stripe. (b) Top view of light sectioning using more than one stripe.

measurement systems which are able to deal with a wide range of parts and can be programmed just by downloading the appropriate 3D CAD data. This would make it obsolete to teach in each new part, however it would require to explicitly calibrate the system.

Stripe projectors are a relatively young means for obtaining a dense 3D surface measurement on a per-pixel basis. Stripe code analysis can be formulated using look-up tables and thus is very fast, with execution times down to a few seconds per 100,000 reconstructed 3D points. However, calibration is often done by using polynomial approximation techniques rather than explicit modelling of interior, additional and exterior parameters. Considering the accuracy levels, flexibiliy, self-diagnosis, and self-calibration possibilities offered by photogrammetric techniques, it is interesting to investigate how photogrammetry can be used to change or even improve upon traditional calibration schemes.

## 2. MEASUREMENT OF DENSE 3D POINT CLOUDS

In case a dense surface measurement is required, several alternative measurement techniques are available. If the object's surface shows sufficient radiometric detail, automatic matching techniques can be employed to recover surface geometry. In most industrial cases, however, surfaces are not very cooperative with respect to texture detail. One method thus uses an artificial static texture pattern projected onto the object by a slide projector.[3,4] Usually, the alternatives concerning the automatic matching procedure are intensity based vs. feature based matching. In intensity based matching, the actual match is not established by a single pixel correspondence, but rather by minimizing grayvalue differences in small windows around the point to be matched. Feature based matching, on the other hand, uses single correspondences of points extracted in a preceding processing step. In order to minimize effects from inaccurate point extraction, a finite element surface reconstruction is applied. Thus, it has to be realized that both intensity based and feature based matching are not well-suited for objects with many surface discontinuities, since those tend to appear smoothed in the reconstructed surface. However, since the underlying measurement principle is strictly photogrammetric, those methods enjoy all the advantages of photogrammetric systems, like the possibility for multiple observations (geometrically constrained matching), self-calibration, robustness and self diagnosis.

On the other extreme, instead of using a static 2D texture pattern, active lighting can just use a single spot, most often generated by a laser beam. Range cameras and laser scanners operating according to this principle use either time-of-flight or phase measurements.[5] Alternatively, active triangulation is possible, where the spacing between outgoing laser beam and position detector lens center forms the triangulation base. Since only a very small spot on the object needs to be illuminated, those systems are often able to scan objects in several meters distance and operate under factory floor lighting conditions. On the other hand, calibration is pretentious due to mechanical tolerances introduced by moving parts such as scanning mirrors, and the depth measurement accuracy may be limited due to a small triangulation base imposed by the mechanical structure of the optical setup.[6] Also, multiple observations from different observation angles are not available.

In-between, light sectioning is a technique that projects lines, or 1D structures, onto the object (see figure 1(a)). The object is then observed by a camera from another viewpoint. Tracking the bright line appearing in the image will yield all parallaxes and thus object depth. To recover the object's 3D geometry, many lines have to be projected under

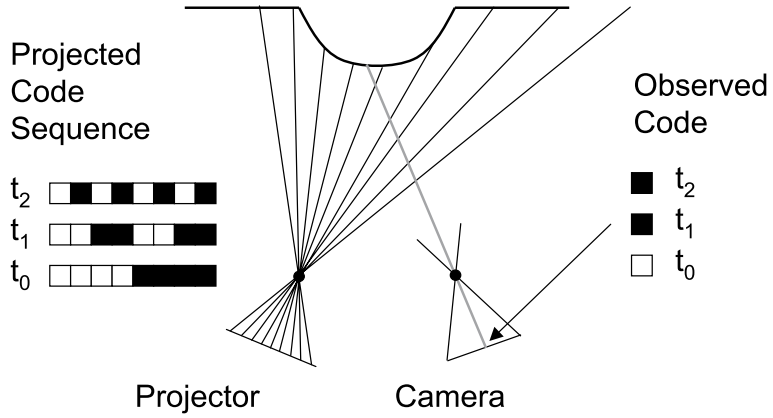


**Figure 2.** Light sectioning using structured light.

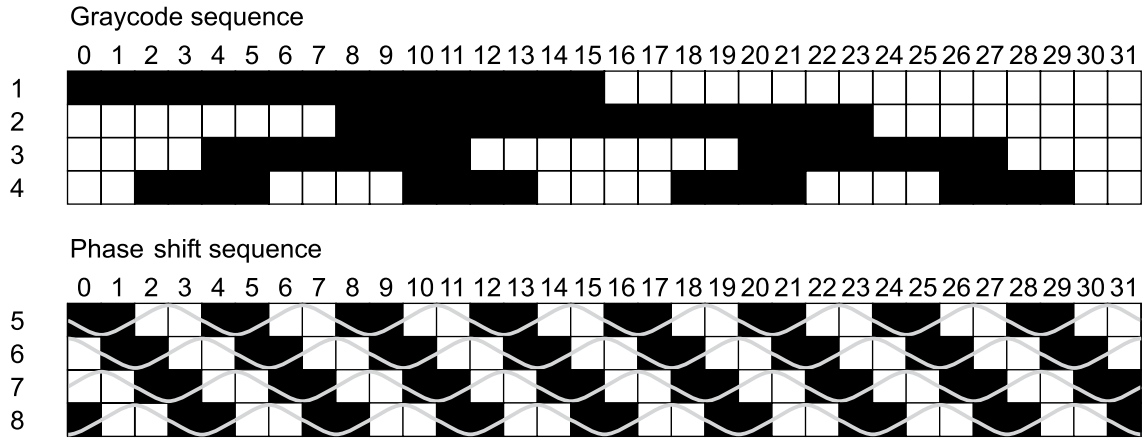


**Figure 3.** Graycode (top) and phase shift (bottom) of a $n = 32$ stripe code sequence. Note the pattern number four which is used to resolve phase ambiguities.

different angles (figure 1(b)), which can be accomplished either by projecting an array of parallel lines simultaneously or by projecting different lines in temporal succession. The first method has the disadvantage that the lines have to be projected closely for a dense reconstruction in which case a correspondence problem arises, especially at steep surfaces or step edges. Projecting in temporal succession means that for $n$ different light section angles $n$ images have to be acquired, where $n$ may be in the order of several hundreds to thousands.

This problem can be solved by the use of structured light techniques, which require only in the order of ld $n$ images in order to resolve $n$ different angles (see figure 2 for $n = 8$). Rather than projecting a single line per image, a binary pattern is used. This technique has been initially proposed by Altschuler.[7,8] Today, different technical realizations of the principle are available, for example using a linear stripe pattern on a glass plate in combination with a cylinder lens,[9] or using a 2D liquid crystal display (LCD) and polarizing filters to switch the lines.[10] Of course, the structured light technique also suffers from some limitations. Due to the fact that the light pattern has to cover an area on the object rather than a single line or a spot, light intensity decreases rapidly with distance. Distances of more than a few meters are not feasible, as is the application under uncontrolled lighting conditions (such as bright sunny outdoor scenes). Also, the original method gives only three observations (light section angle and image coordinates) for each 3D point to be determined, so there is no redundancy and no accuracy assessment is possible.

## 3. STRIPE PROJECTION

### 3.1. Structured Light and Phase Shift

For structured light analysis, projecting the Graycode is superior to a binary code projection (see figure 3, top). On the one hand, successive numbers of the Graycode vary exactly in one bit. Thus, wrong decoding which is most likely to occur at locations where one bit switches, introduces only a misplacement of at most one resolution unit. On the other hand, the width of bright and dark lines in the pattern with finest resolution is twice as wide compared to the binary code. This faciliates analysis especially at steep object surfaces where the code appears to be compressed.

To obtain a resolution beyond the number of lines which can be switched by the projector, phase shifting can be applied. This uses the on/off intensity pattern generated by the switched projector lines as an approximation of a sine wave. The pattern is then shifted in steps of $\pi/2$ for a total of $N = 4$ pattern positions. Approximating the sampled values $f(\phi_i)$ at a certain fixed position (figure 3, bottom) by

$$\begin{aligned} C \cdot \cos(\phi - \phi_0) &= C \cdot \cos\phi_0 \cos\phi + C \cdot \sin\phi_0 \sin\phi \\ &= A \cdot \cos\phi + B \cdot \sin\phi \end{aligned}$$

where the coefficients $A$ and $B$ can be determined from Fourier analysis by

$$A = \frac{2}{N} \sum_{i=0}^{N-1} f(\phi_i) \cos\phi_i \text{ and } B = \frac{2}{N} \sum_{i=0}^{N-1} f(\phi_i) \sin\phi_i$$

a phase shift $\phi_0 = \arctan(B/A)$ is obtained, which in our case ($N = 4$, $\phi_i = \{0, \pi/2, \pi, 3\pi/2\}$) simplifies to

$$\phi_0 = \arctan \frac{f_1 - f_3}{f_0 - f_2} \,.$$

To estimate errors we anticipate in phase computation, we assume that the intensity of the phase shift pattern can be approximated by

$$f(C, D, \phi_0) = C \cdot \cos(\phi - \phi_0) + D$$

where $C$, $\phi_0$ and $D$ are the unknown values for amplitude, phase shift and offset, respectively. Least squares parameter estimation uses four observation equations

$$g_i + v_i = C \cdot \cos(\phi_i - \phi_0) + D$$

where again $\phi_i = \{0, \pi/2, \pi, 3\pi/2\}$. Assuming intensity measurements to be uncorrelated, we set the cofactor matrix $Q_g = \text{diag}\left(\sigma_g^2, \ldots, \sigma_g^2\right)$ ($\sigma_g^2$ being the variance of the grayvalue noise) and, since $A^T A = \text{diag}\left(4, 2, 2C^2\right)$ is a diagonal matrix, we finally obtain

$$\sigma_{\phi_0} = \frac{\sigma_g}{\sqrt{2}C} \,.$$

Thus, if we assume $\sigma_g = 2$ and $C = 25$ (which corresponds to a modulation of 50), $\sigma_{\phi_0} = 0.057$. Since 4 projector lines are used for the range $[0, 2\pi]$ (figure 3), this transforms to 0.036, or 1/28 of the line width. This means that subpixel measurements should be feasible which are comparable in accuracy to photogrammetric measurements. However, it has to be taken into account that nonuniform object surface properties, such as a sharp change from black to white result in systematic measurement errors. Also, since the camera pixels effectively integrate over a certain area of the stripe code, the above error estimation is only true with a camera resolution sufficiently higher than the projector resolution.

### 3.2. Stripe Projectors

We used a LCD type projector for our experiments.[11] The line pattern is generated by switching lines on a two-dimensional LCD backlit from behind (figure 4(a)). This type of projector has the advantage that there are no moving parts. On the other hand, due to the LCD with polarizing filters, brightness is inferior to projectors using metal coated glass plates.

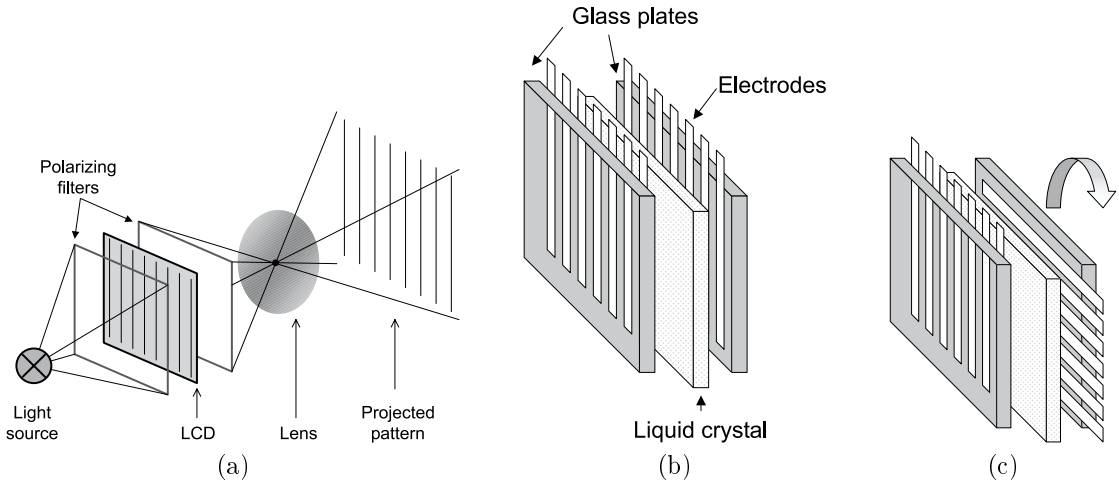


**Figure 4.** (a) Stripe projection using a two-dimensional LCD. (b) Normal type LCD. (c) Cross-pattern LCD. The second glass plate is turned by 90 degrees.

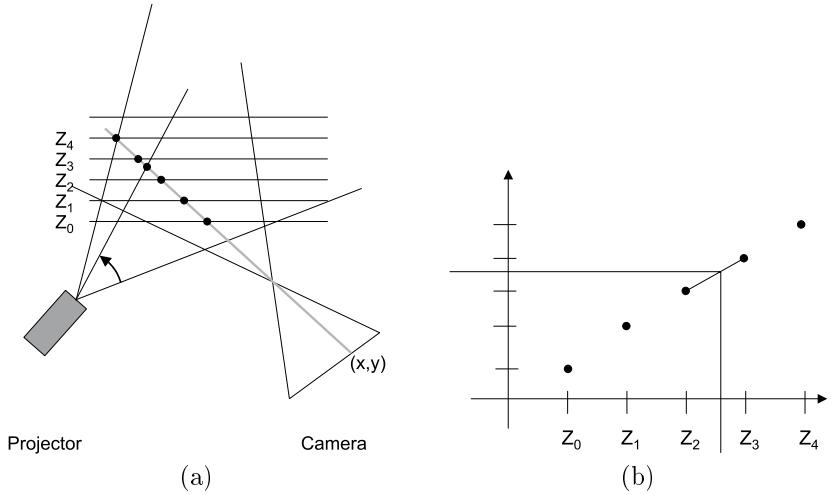


**Figure 5.** (a) Polynomial depth calibration using a plane at different distances $Z_i$. For each pixel, calibration yields a table of values $\phi_i$. (b) $(Z_i, \phi_i)$ pairs and lookup of a value $Z$ for a given $\phi$ during measurement.

While normal LCD stripe projectors use two glass plates with conducting stripes aligned precisely (figure 4(b)), a cross-pattern projector has one of the glass plates turned by 90 degrees (figure 4(c)). Since all stripes can be switched individually, arbitrary vertical and horizontal stripe patterns can be generated (albeit no arbitrary 2D patterns can be generated, since the 2D pattern always results from a XOR of the two line patterns). In the context of a photogrammetric evaluation, this means that the projector can be modeled as an inverse camera delivering 2D "image" coordinates. On the down side, twice as many stripe patterns have to be projected per sequence in order to obtain $x$ and $y$ coordinates.

## 4. CALIBRATION

### 4.1. Polynomial Calibration Model

One standard approach for calibrating coded light sensors is polynomial depth calibration. A plane is positioned successively at different distances $Z$ from the projector/camera setup (figure 5(a)). Usually, the nearest and furthest plane delimit the volume which is later to be used for measurements. The values $Z_i$ are often chosen equidistantly and have to be known to a high accuracy. Considering one single pixel of the camera, each depth $Z_i$ will yield

a corresponding absolute phase angle $\phi_i$ (combined from Graycode and phase shift). The table of measured pairs $(Z_i, \phi_i)$ can then be used to estimate an approximating function, like a polynomial function $Z = Z(\phi)$ (figure 5(b)). During measurement, $Z$ depth is computed for each pixel by first decoding absolute phase, followed by the evaluation of the (pixel-specific) approximation function $Z = Z(\phi)$. The $X$ and $Y$ coordinates may then be recovered using the camera exterior orientation.

In order to speed up evaluation, $Z = Z(\phi)$ may also be approximated by a piecewise linear function. In this case, all $(Z_i, \phi_i)$ pairs are stored in a table (i.e. one table entry per pixel and per depth $Z_i$. $Z$ is is interpolated, for example by linear interpolation, from $Z_i$ and $Z_{i+1}$, if $\phi_i \leq \phi \leq \phi_{i+1}$.

Polynomial depth calibration suffers from practical and accuracy limitations. First, the values $Z_i$ used during calibration have to be very accurate. A precise z-stage can be used for this. However, this will limit the measurement volume. Also, since z stages are expensive, users may be unable to calibrate the sensor to sufficient accuracy, so factory calibration becomes necessary. In this case, it is problematic to guarantee the stability of the relative orientation between projector and camera (especially for larger base distances).

Additionally, since each pixel is treated individually, phase decoding errors during calibration lead to wrong approximation functions. This problem may be alleviated by the smoothing introduced by the approximation function (exploiting coherency in $Z$) or by applying lowpass filtering to the phase images (exploiting coherency in $X$ and $Y$).

Despite those drawbacks, polynomial depth calibration lends itself nicely to a (fast) lookup-table implementation. Performance is an important factor in stripe projection analysis, since object coordinates $(X, Y, Z)$ have to be computed for each pixel of the camera, i.e. several $100,000$ times for one depth image.

### 4.2. Photogrammetric Calibration

Since the projector is able to project cross patterns, it can be modeled as an inverse camera. Compared to normal stripe projectors, $x$ *and* $y$ "image" coordinates can be obtained from decoding the absolute phase $\phi_x$ and $\phi_y$. Thus, the projector can be calibrated using a planar testfield and a convergent setup. Using white dots on a black background, image coordinates for the camera are obtained in the usual way, e.g. by computing the weighted centroid. Corresponding projector coordinates are then computed from the $\phi_x$ and $\phi_y$ phase images by a sampling at this centroid position.

We used a camera model with six additional parameters for the bundle solution.[12] The parameters are $A_1$, $A_2$ for the radial symmetric distortion, $A_3$, $A_4$ for scale and shear and $A_5$, $A_6$ for decentering distortion. The parameters are applied in the order

$$\begin{aligned} x' &= x + xA_1(r^2 - r_0^2) + xA_2(r^4 - r_0^4) + 2A_5xy + A_6(r^2 + 2x^2) + x_0 \\ y' &= y + yA_1(r^2 - r_0^2) + yA_2(r^4 - r_0^4) + 2A_6xy + A_5(r^2 + 2y^2) + y_0 \\ x'' &= x' + A_3x' + A_4y' \\ y'' &= y' + A_4x' - A_3y' \end{aligned}$$

where $(x, y)$ are image coordinates obtained from applying the collinearity equation, $(x_0, y_0)$ is the principal point, $r = \sqrt{x^2 + y^2}$ is the pixel radius and $r_0$ is usually set to $2/3$ of the image radius.

## 5. EXPERIMENTS

### 5.1. Experimental Setup

We used a printed testfield glued to a ceramic tile (note that plane planarity is not a prerequisite for photogrammetric calibration, so any tile can be used provided it is mechanically stable). The testfield consisted of $13 \times 19$ white targets on a black background (figure 6(a)).

The projector we used features a LCD with $640 \times 640$ lines, line spacing of $90\mu$m (LCD size $57.6^2$ mm$^2$), and a halogen light source of 400W.[10] Patterns can be switched in 14 milliseconds making it feasible to acquire images in video realtime, although we did not use this option since it requires hardware support. Commands and pattern sequences can be sent to the projector via a RS-232 interface.

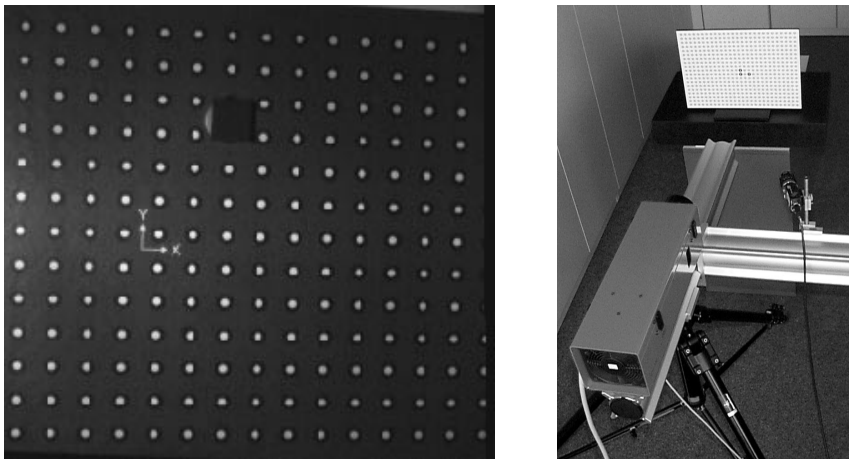

(a) (b)

**Figure 6.** (a) Testfield as seen by the camera. (b) Setup consisting of projector, camera and testfield.

| | camera | projector |
|---|---|---|
| total $x$ residual | 0.28$\mu$m | 7.66$\mu$m |
| total $y$ residual | 0.24$\mu$m | 9.90$\mu$m |
| $\sigma_X$ (RMS) | 7.8$\mu$m | 15.2$\mu$m |
| $\sigma_Y$ (RMS) | 6.2$\mu$m | 19.6$\mu$m |
| $\sigma_Z$ (RMS) | 20.1$\mu$m | 55.4$\mu$m |

**Table 1.** Image residuals and accuracy estimates for the camera and projector calibration (note camera pixels are 8$\mu$m and projector "pixels" are 90$\mu$m).

The camera we used was a standard video camera (SONY XC75) with a $1/2''$ imager and approximately 8$\mu$m pixel size, grabbed with an ELTEC frame grabber at $748 \times 576$ pixels. Projector and camera were mounted on a stable aluminium profile with a fixed relative orientation (figure 6(b)).

For the photogrammetric calibration, we moved the testfield in front of the projector/camera setup to obtain a total of 20 images in a highly convergent configuration. Since we did not use coded targets, image measurement was done semiautomatic, where approximate coordinates for 4 targets had to be picked in each image in order to measure automatically all image coordinates. Coordinate measurement was done by weighted centroid and projector coordinates were obtained by bilinear interpolation in the phase images at the centroid position.

We first did a separate calibration for the camera and projector. Table 1 lists the results in terms of image residuals and accuracy estimates for the object coordinates. Then, we calibrated both the projector and camera in a single bundle run (i.e. 40 stations with a total of 6656 observed image points). The interior orientations obtained from this bundle adjustment are shown in table 2.

For the polynomial depth calibration, we used the standard procedure suggested by the projector manufacturer. Since no z-stage was available, the manufacturer provided us with a calibration device which can be bought by customers who wish to calibrate their sensor. This device is made from aluminium with matte black finish. A printed testfield of size $297 \times 420\text{mm}^2$ is glued on top of a planar plate, which can be locked at different depths. The lock positions are defined by several holes drilled by a CNC machine to a high accuracy.

To calibrate, the plane was positioned at 11 different depths with a spacing of 10 mm. Thus, the calibration covers a depth range of 10 cm. The software provided with the stripe projector is able to calibrate the projector from those images fully automatically.

### 5.2. Accuracy Assessment

In order to verify both calibrations, we used a plane-table as calibration normal. This table is certified to have an overall surface flatness of 7 microns. Since the surface is black, we covered it by a self-adhesive white foil to obtain a

| | camera | | projector | |
|---|---|---|---|---|
| $x_0$ | -0.081293 | (0.0029) | 1.178883 | (0.0580) |
| $y_0$ | -0.114492 | (0.0028) | 0.331241 | (0.0596) |
| $c$ | 12.102765 | (0.0034) | 181.915599 | (0.0667) |
| $A_1$ | $-0.603793 \cdot 10^{-03}$ | $(0.1176 \cdot 10^{-06})$ | $0.555660 \cdot 10^{-06}$ | $(0.1176 \cdot 10^{-06})$ |
| $A_2$ | $0.308968 \cdot 10^{-05}$ | $(0.8361 \cdot 10^{-10})$ | $-0.266407 \cdot 10^{-09}$ | $(0.8361 \cdot 10^{-10})$ |
| $A_3$ | $-0.143177 \cdot 10^{-01}$ | $(0.1717 \cdot 10^{-04})$ | $0.200536 \cdot 10^{-03}$ | $(0.1717 \cdot 10^{-04})$ |
| $A_4$ | $0.308307 \cdot 10^{-04}$ | $(0.1702 \cdot 10^{-04})$ | $0.133679 \cdot 10^{-03}$ | $(0.1702 \cdot 10^{-04})$ |
| $A_5$ | $-0.121978 \cdot 10^{-03}$ | $(0.6954 \cdot 10^{-06})$ | $0.204489 \cdot 10^{-05}$ | $(0.6954 \cdot 10^{-06})$ |
| $A_6$ | $-0.757670 \cdot 10^{-04}$ | $(0.6632 \cdot 10^{-06})$ | $0.980716 \cdot 10^{-05}$ | $(0.6632 \cdot 10^{-06})$ |

**Table 2.** Interior orientation for the projector and the camera. Accuracy estimates are in brackets. $c$ is the focal length. $x_0$, $y_0$ and $c$ are given in millimeters.

| plane angle | photogrammetric calibration | | polynomial depth calibration | |
|---|---|---|---|---|
| (degrees) | r.m.s. | maximum | r.m.s. | maximum |
| 0 | 0.031 | 0.174 | 0.036 | 0.162 |
| -15 | 0.040 | 0.275 | 0.031 | 0.150 |
| 10 | 0.041 | 0.268 | 0.036 | 0.304 |
| 20 | 0.043 | 0.177 | 0.033 | 0.180 |

**Table 3.** Deviations of measured 3D points from a fitted plane (in millimeters).

high signal modulation. The plane-table was positioned in front of the sensor both perpendicular to the optical axis and at different angles. Images were taken and evaluated independently using the polynomial depth calibration and the photogrammetric calibration.

Photogrammetric 3D point determination was carried out using a forward intersection based on the exterior orientation, interior orientation and additional parameters obtained from the bundle. Forward intersection usually uses 4 observed image coordinates to estimate 3 world coordinates. However, if only three observations are used, no cross patterns need to be projected. Thus, image capture can be twice as fast (omitting e.g. all horizontal stripe projections), while projector calibration still can be carried out using cross patterns to obtain maximum accuracy. The drawback in this case is that there is no redundancy in estimating 3D world coordinates during the measurement. 3D point determination according to the depth calibration was implemented using the software supplied by the projector manufacturer.

After a dense cloud of measured 3D points is obtained, a plane is fit to the data and minimum, maximum and standard deviation are determined. Table 3 shows the results of this step. From this table, we can see that both approaches yield similar accuracy values. Polynomial depth calibration is slightly superior (10 microns in r.m.s.), albeit it can be used only for the calibrated measurement volume (10 centimeters in depth). 40 microns in r.m.s. translates to approximately $1:5000$ relative accuracy.

## 6. CONCLUSION AND OUTLOOK

In this paper, we have compared a polynomial depth calibration to a photogrammetric calibration. As a conclusion, we can say that both calibrations yield comparable accuracies. However, polynomial depth calibration needs an accurate planar calibration device whereas photogrammetric calibration can use any geometrically stable testfield. In our opinion, it is also an advantage to have exterior and interior orientations explicilty. First, this will give the possibility to design an online exterior orientation module, so problems encountered frequently with changing exterior orientations can be circumvented. Second, the orientations hold true for all depths, so there are less problems with measured points lying outside the original volume covered by a polynomial depth calibration.

In the future, we will enhance our sensor setup by two high resolution digital cameras. This will reduce errors introduced by the analog video signal transmission and will allow to measure phase angels more precisely. Also, if more than one camera is used, several configurations can be tested. For example, the projector might be used to

solve the correspondence problem of two cameras without actually providing image coordinate observations. Also, it will be interesting to combine image matching techniques with the coded light approach.

## ACKNOWLEDGEMENTS

The support of the German Science Foundation is gratefully acknowledged.

## REFERENCES

1. A. Grün, "Digital close-range photogrammetry — progress through automation," in *Proc. Comm. V Symp. Close Range Techniques and Machine Vision, IAPRS, vol. 30, part 5*, pp. 122–135, 1994.
2. C. S. Fraser, *Close Range Photogrammetry and Machine Vision*, ch. 12. Whittles Publishing, UK, 1996.
3. T. Kludas, "Three dimensional surface reconstruction with the Zeiss photogrammetric industrial measurement system InduSURF digital," in *IAPRS Vol. 30 Part 5W1*, E. P. Baltsavias, ed., pp. 285–291, 1995.
4. P. Kludas and F. Petran, "Automatic reconstruction of concept models by using a digital photogrammetric measurement system," in *IAPRS Vol. 30 Part 5W1*, E. P. Baltsavias, ed., pp. 176–185, 1995.
5. A. Wehr, *Entwicklung und Erprobung von opto-elektronischen Entfernungsmeßsystemen mit CW-Halbleiterlasern*. PhD thesis, Universität Stuttgart, 1991.
6. J.-A. Beraldin, S. F. El-Hakim, and L. Cournoyer, "Practical range camera calibration," in *SPIE vol. 2067, Videometrics II*, pp. 21–31, 1993.
7. M. Altschuler, B. R. Altschuler, and J. Taboada, "Measuring surfaces spacecoded by a laser-projected dot matrix," in *SPIE vol. 182, Imaging Applications for Automated Industrial Inspection and Assembly*, 1979.
8. T. G. Stahs and F. M. Wahl, "Fast and robust range data acquisition in a low-cost environment," in *Close-Range Photogrammetry meets Machine Vision, SPIE Vol. 1395*, pp. 496–503, 1990.
9. Breuckmann GmbH, Torenstraße 13, Meersburg, Germany, *Topometrisches 3D-Meßsystem, Technische Beschreibung*.
10. ABW, *ABW 640 Bedienungsanleitung*. ABW, Gutenbergstraße 9, 72636 Frickenhausen, 1997.
11. H. Wolf, "Vergleichende Betrachtung der verschiedenen strukturierten Lichtquellen von ABW," in *Proc. second ABW workshop*, ABW, 1996.
12. G. Technet GmbH, Berlin, *PICTRAN-B version 2.2.00 User's Guide*, 1995.